ARTICLE NO. 78-1022R

Installed Performance of Vectoring/Reversing Nonaxisymmetric Nozzles

P. E. Hiley,* D. E. Kitzmiller,† and C. M. Willard‡
McDonnell Douglas Corporation, St. Louis, Mo.

An experimental program was conducted to determine the internal and installed performance characteristics of five different thrust vectoring and reversing nonaxisymmetric nozzle concepts for tactical fighter aircraft. As part of this program, the nonaxisymmetric nozzles and an advanced axisymmetric baseline nozzle were tested in the AEDC 16-ft transonic Propulsion Wind Tunnel at Mach numbers from 0.4 through 1.5. The twin-nozzle models were mounted to a partially metric jet-effects model, with nozzle exits located at the trailing edge of a fighter wing planform. Tests were conducted at three unvectored power settings, thrust vector angles up to 30 deg and dry power reverse thrust. Nozzle pressure ratios were varied about nominal values for an advanced turbofan engine cycle at each test Mach number. At unvectored conditions, the nonaxisymmetric nozzles with external expansion surfaces exhibited the highest thrust-minus-drag at both cruise and maneuver conditions. Performance was equal to or better than that of the axisymmetric baseline nozzle. Vectoring was found to improve the lift-to-drag ratio for all nonaxisymmetric nozzles at all positive thrust vector angles. The lift, drag, and pitching moment increments associated with vectoring were shown to correlate well with modified trailing edge flap theory. Reverse thrust levels equalled 50% of forward, dry power thrust at static conditions, with a reversing effectiveness nearly twice this value demonstrated at Mach 0.9.

Nomenclature

b_N = effective nozzle span, including interfairing for close-spaced twin nozzles
C_D = drag coefficient, D/qS_w
C_{F_g} = nozzle resultant gross thrust coefficient, F_g/F_i
$C_{(F_g-D)}$ = normalized thrust-minus-drag coefficient at $\alpha=0$ deg and $\delta_N=0$ deg, $(F_g-D)/F_i$
C_L = lift coefficient, L/qS_w
C_m = pitching moment coefficient, $PM/qS_w\bar{c}$
C_T = aerodynamic thrust coefficient, F_g/qS_w
C_{T-D} = normalized thrust-minus-drag coefficient, $(T-D)/qS_w$
$\bar{c}$ = wing mean aerodynamic chord (13.91 in.)
c_{EFF} = effective local wing section chord in nozzle proximity
D = drag force (pressure and friction) of complete wing/aftbody/nozzle, unless noted
F_i = nozzle ideal thrust for complete isentropic expansion of actual jet flow to ambient static pressure
F_g = measured resultant nozzle gross thrust
h_N = nozzle exit height
$K_{L,D \text{ or } M}$ = empirically derived correlation constants
L = lift force of complete wing/aftbody/nozzle, unless noted
M = freestream Mach number
NPR = ratio of nozzle total to freestream ambient pressures
PM = pitching moment of complete wing/aftbody/nozzle, resolved about $0.25\bar{c}$ location unless otherwise noted
q = freestream dynamic pressure
S_w = wing reference area (454 in.^{2})
T = gross thrust force resolved into flight path direction
X_N = axial distance from leading edge of c_{EFF} to gross thrust vector point of application
$X_{0.25c_{EFF}}$ = axial distance from leading edge to 25% location on c_{EFF}
X_Γ = axial distance from leading edge of c_{EFF} to effective application point of induced lift
α = angle of attack
β = nozzle final boattail angle
Δ = incremental value
δ_N = nozzle geometric turning angle (downward flow direction positive)
δ_V = nozzle measured thrust vector angle

Subscripts

AERO = aerodynamic forces or moments (direct jet contributions removed)
i = induced, refers to lift-induced drag
N = nozzle, or nozzle exit location
R = reverse thrust
REF = reference conditions
TOT = total forces or moments (aerodynamic plus direct jet contributions)
Γ = thrust-vector-induced aerodynamic force or moment increments referenced to unvectored, jet-on conditions

Introduction

NONAXISYMMETRIC exhaust nozzles have recently been shown to provide internal performance competitive with axisymmetric nozzles both statically[1] and under simulated flight conditions.[2] This is in addition to the benefits of installed drag reduction[3,4] and favorable aerodynamic effects[4-6] induced by vectoring of the jet. Effective vectoring and reversing capabilities also can be incorporated with less complexity.[7]

Presented as Paper 78-1022 at the AIAA/SAE 14th Joint Propulsion Conference, Las Vegas, Nev., July 25-27, 1978; submitted Oct. 27, 1978; revision received April 10, 1979.

Index categories: Aerodynamics; Airbreathing Propulsion; Jets, Wakes, and Viscid-Inviscid Flow Interactions.

*Section Chief-Technology.
†Engineer-Technology. Member AIAA.
‡Lead Engineer-Technology.

In order to provide a sound data base for future evaluation of nonaxisymmetric nozzles, an experimental program was conducted in the transonic Propulsion Wind Tunnel (PWT-16T) at Arnold Engineering Development Center (AEDC) in Tennessee. Major test objectives were to determine the thrust-minus-drag characteristics of several nonaxisymmetric nozzle installations at unvectored and reverse-thrust conditions, and the effects of thrust vectoring on the external aerodynamics (supercirculation). The purpose of this paper is to present the results of this wind-tunnel investigation. A summary of results for the complete program under which these tests were conducted can be found in the final report.[8]

Five nonaxisymmetric, or two-dimensional (2-D) nozzles were tested to satisfy the test objectives, representing first generation, low aspect ratio designs furnished by the engine companies (Fig. 1). Three generically different types of 2-D nozzles were included: 1) 2-D convergent-divergent (2-D C-D) with internal expansion only, 2) 2-D single expansion ramp with combined internal/external expansion, and 3) 2-D plug with combined internal/external expansion. An axisymmetric C-D nozzle also was tested to serve as a baseline for comparison.

A 2-D C-D design with vectoring and reversing capabilities was furnished by both General Electric (GE) and Pratt and Whitney Aircraft (P&WA). The GE Augmented Load Balanced Exhaust Nozzle (ALBEN) is a vectoring derivative of the Augmented Deflector Exhaust Nozzle (ADEN)[9] single expansion ramp concept. Two 2-D plug nozzles were designed by P&WA. The P&WA/MCAIR Variable Incidence Plus (VIP) has vectoring only, and the P&WA/NASA plug design includes both vectoring and reversing. The axisymmetric baseline nozzle design with no vectoring or reversing was furnished by P&WA.

In this paper, the model and test program are described, and the test results are presented at unvectored, vectored, and reverse-thrust conditions.

Model Description

A jet-effects model used in several NASA-Langley programs[4-6] provided the common Test Pod for all nozzle configurations. A tandem balance system was used (Fig. 2) with the metric nozzles isolated through a pair of metal bellows flow-transfer assemblies. The main balance measured the combined lift, drag, and pitching moment due to the nozzle gross thrust and the lift, drag, and moment on the model aftbody, wing, and nozzle boattail/interfairing. The piggyback thrust balance measured the forces and moments due to the gross thrust, and the forces and moments occurring on the nozzle boattail/interfairing, providing added data visibility. A total of 52 pressure taps located on the boattail of one nozzle and the interfairing between the nozzles made it possible to separate (at wind-on conditions) the internal gross thrust from the external forces and moments.

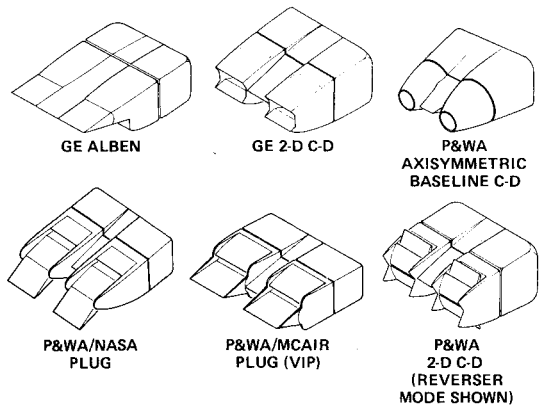

Fig. 1 Nonaxisymmetric and axisymmetric nozzle models.

Table 1 Installed performance summary[a]

Nozzle	C_{F_g}	$C_{(F_g - D)}$
ALBEN	0.996	0.761
VIP	0.999	0.751
GE 2-D C-D	0.979	0.730
P&WA 2-D C-D	0.980	0.725
Axi baseline	0.988	0.759

[a] Dry power, Mach 0.9, $\alpha = 0$, $NPR = 3.5$.

Test Program

The test program is summarized in Fig. 3. All of the 2-D nozzles were tested at both vectored and unvectored conditions with the low Mach A/B power setting at Mach numbers of 0.6, 0.9 and 1.5. Vectoring at dry and high Mach

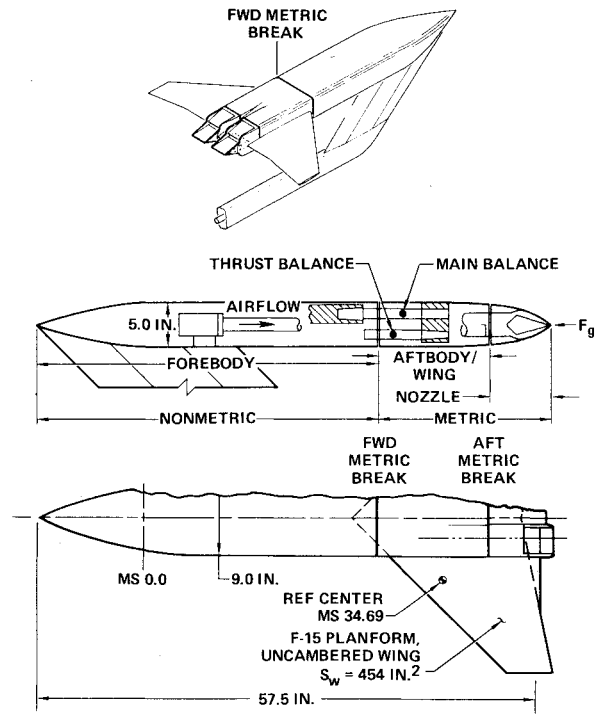

Fig. 2 NASA Test Pod model.

NOZZLE CONFIGURATION	POWER SETTING	VECTORED (1)	REVERSE	MACH NUMBERS 0	0.4	0.6	0.9	1.2	1.5
P&WA/MCAIR VIP	DRY	X		X		X	X		
	LM A/B	X		X	X	X	X	X	X
	HM A/B	X		X			X	X	X
P&WA/MCAIR VIP, WINGS OFF	LM A/B	X		X		X	X		X
P&WA/NASA PLUG	LM A/B	X		X		X	X		X
P&WA 2-D C-D	DRY		X	X		X	X		X*
	LM A/B	X		X		X	X		X
	HM A/B			X			X		X
GE 2-D C-D	DRY		X	X		X	X	X*	X*
	LM A/B	X		X		X	X	X	X
	HM A/B			X			X		X
GE ALBEN	DRY	X		X			X	X	
	LM A/B	X		X	X	X	X	X	X
	HM A/B	X		X			X	X	X
AXI BASELINE	DRY			X	X	X	X		
	LM A/B			X	X	X	X	X	X

NPR RANGE (WIND-ON)

MACH	NPR
0.4, 0.6	1 → 5
0.9	1 → 7
1.2, 1.5	1 → 9

α RANGE (JET-ON)

MACH	α
0.4 → 0.9	0 → 16
1.2, 1.5	0 → 12

*REVERSER ONLY.

(1) ALL POWER SETTINGS TESTED UNVECTORED.

Fig. 3 Test matrix.

afterburning settings also was accomplished for the ALBEN and VIP nozzles. Thrust vector angles up to 30 deg and angles of attack from −2 through 16 deg were tested. The 2-D C-D nozzles were tested in the reverse-thrust mode up to Mach 1.5.

Unvectored Installed Performance

Unvectored installed performance (thrust minus drag) was determined up to 16 deg angle of attack for all 2-D nozzle installations at dry and low Mach afterburning power. A design point summary at Mach 0.9, dry power, and zero degrees angle of attack is shown in Table 1, giving the wind-on internal performance (C_{F_g}) as well as the installed performance [$C_{(F_g-D)}$]. Installed performance of the external expansion nozzle types was essentially the same as the axisymmetric baseline nozzle installation. The 2-D C-D nozzles were as much as 3.5% lower, however, attributable to nozzle drag levels higher than the baseline axisymmetric nozzle.

To evaluate the lower 2-D C-D performance, the relative pressure drags on the nozzle boattail and interfairing were evaluated. The boattail pressure drags were computed from the 40 pressure taps on the nozzle boattail flaps and sidewall downstream of the aft metric break on the Test Pod. The interfairing pressure drags were computed from the 12 pressure taps on the wedge-shaped fairing between the nozzles downstream of the aft metric break. The boattail and interfairing pressure drags are shown in Fig. 4 at the Mach 0.9, dry power design point condition. The boattail drags of the 2-D C-D nozzles, as well as the VIP, were considerably higher than the ALBEN and axisymmetric nozzle drags. This is because the boattail angles are about 10 deg higher on the 2-D C-D and VIP nozzles. The interfairing drags of the 2-D C-D nozzles also were higher than the axisymmetric and ALBEN levels, as seen in the lower portion of Fig. 4. Inspection of the interfairing pressure distributions revealed flow separation near the trailing edge for both 2-D C-D nozzle installations. The 2-D C-D interfairing had the highest flow angles, because of a short fairing length. The shorter length was dictated by full-scale considerations which led to terminating the fairing at the beginning of the cutback sidewall.

At afterburning power, installed performance for the five nozzles was essentially equivalent to the axisymmetric baseline nozzle at subsonic conditions and generally superior supersonically. The performance levels at Mach 0.9 and 1.5 are summarized in Table 2. At Mach 0.9, both internal and installed performance were within ±1% of the axisymmetric nozzle. However, at Mach 1.5, the installed performance for the external expansion nozzles was 2-3% higher, even though internal performance was essentially equal. This is attributed to improved wave drag characteristics, resulting from more favorable area distributions. For the plug-type nozzles and the ALBEN (a "half-plug"), the rate of aftbody area change is decreased by the presence of the external expansion surfaces. Further, cross-sectional area terminates abruptly at the wing

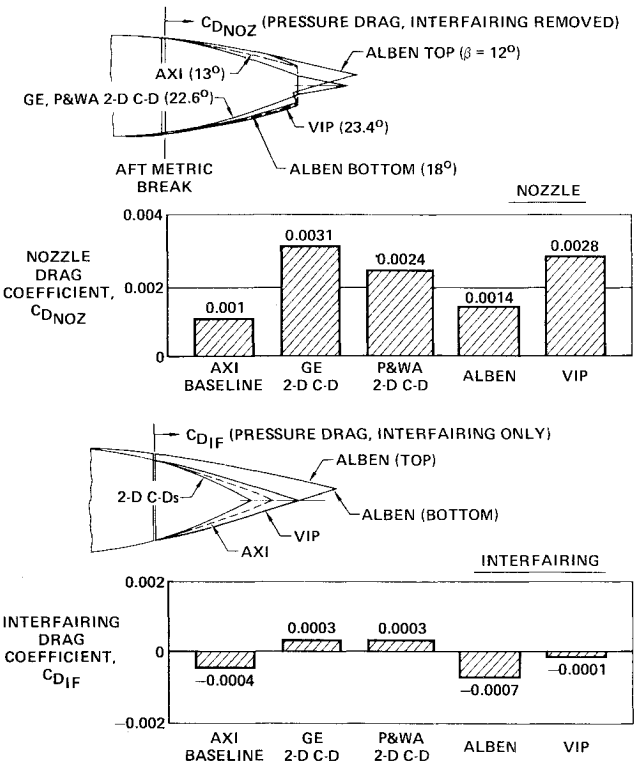

Fig. 4 Nozzle and interfairing drag comparisons (dry power, Mach 0.9, $NPR = 3.5$, $\delta_N = 0$ deg).

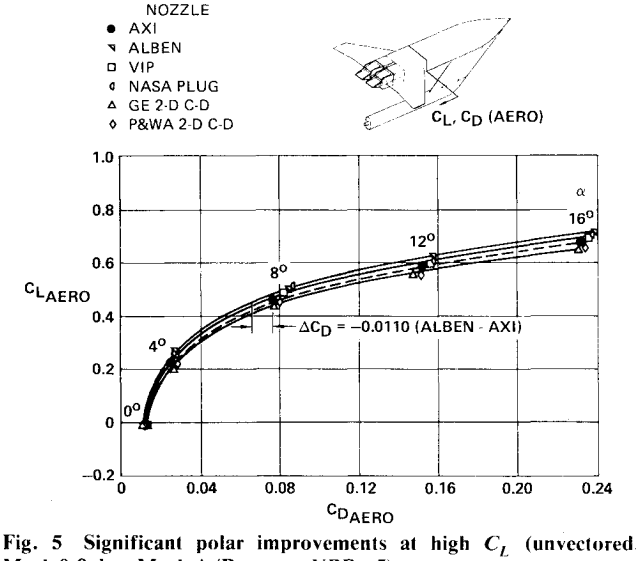

Fig. 5 Significant polar improvements at high C_L (unvectored, Mach 0.9, low Mach A/B power, $NPR = 5$).

Table 2 Installed performance summary[a]

Mach	*NPR*	Nozzle	C_{F_g}	$C_{(F_g-D)}$
0.9	5.0	ALBEN	0.981	0.915
		NASA plug	0.984	0.914
		VIP	0.968	0.906
		GE 2-D C-D	0.989	0.904
		P&WA 2-D C-D	0.986	0.895
		Axi baseline	0.989	0.903
1.5	9.0	ALBEN	0.973	0.775
		NASA plug	0.971	0.776
		VIP	0.962	0.783
		GE 2-D C-D	0.972	0.756
		P&WA 2-D C-D	0.966	0.753
		Axi baseline	0.971	0.755

[a] Low Mach A/B power, $\alpha = 0$ deg.

trailing edge for the C-D nozzles, but continues downstream to the end of the expansion surfaces for the ALBEN installation.

At unvectored maneuver conditions, polar improvements from the axisymmetric baseline at high angles of attack were observed for the two plug installations and particularly for the ALBEN (Fig. 5). Both 2-D C-D nozzles had somewhat poorer unvectored performance than the axisymmetric baseline nozzle.

It is important to note that the forebody lift and drag were not measured by the balance system. In performance comparisons, therefore, reference must be made to typical maneuver angles of attack rather than lift coefficient. As indicated on Fig. 5, for example, the drag reduction of the ALBEN from the axisymmetric baseline nozzle at $\alpha = 8$ deg

(same C_L value) is $\Delta C_D = 0.0110$. This would represent a 13% drag reduction for a typical current fighter at this angle of attack.

The indicated improvement in lift to drag ratio (L/D) is due to better drag due to lift (C_{D_i}) characteristics of the ALBEN. This advantage is particularly prevalent at Mach 0.9, where there is a beneficial interaction between the wing and body. These observations are illustrated in Fig. 6, where the difference in drag-due-to-lift between the ALBEN and axisymmetric nozzles is shown for the wing/body and body alone.

Vectored Installed Performance

Vectored Performance

When the gross thrust is vectored at any angle of attack, the thrust components are changed according to the following equations:

$$\Delta\text{Jet Lift} = C_{T_{\delta_v}} \sin(\alpha+\delta_v) - C_{T_{\delta_v}} = 0 \text{ deg}^{(\sin\alpha)}$$

$$\Delta\text{Thrust Loss} = C_{T_{\delta_v}} [1-\cos(\alpha+\delta_v)] - C_{T_{\delta_v}} = 0 \text{ deg}^{(1-\cos\alpha)}$$

$$\text{Jet Moment} = C_{T_{\delta_v}} \sin(\delta_v)\,(X_N - X_{0.25\bar{c}})/\bar{c}$$

where

$$(X_N - X_{0.25\bar{c}})/\bar{c} = 0.78$$

The effect of the vectored thrust has been found to induce increments in lift, drag, and pitching moment on the adjacent body and the airfoils. The trend has been for the thrust vector to induce a positive lift increment (C_{L_Γ}) due to increased circulation (supercirculation) on the wing/body. Typically, the increased lift is accompanied by large nose-down pitching moment increments (C_{m_Γ}). The vector-induced effects on drag (C_{D_Γ}) have varied widely, ranging from drag reduction due to vectoring to significant drag increases. It would be expected, however, that a vector-induced lift increase would be accompanied by an increase in drag (drag-due-to-lift). The question is whether or not vectoring can improve the overall L/D.

Typical vectoring effects from this program are shown in Fig. 7, demonstrating significant supercirculation lift (C_{L_Γ} three times jet lift, and large nose-down moments). As expected, drag increases also were induced. Note that all induced increments are referenced to the jet-on, undeflected nozzle condition and thereby do not reflect the effect of turning the jet on. Any such vectored jet effects, or throttle-dependent increments, could be treated separately in a thrust/drag accounting procedure.

The lift/drag changes due to vectoring must be combined with the changes in the magnitude of the gross thrust vector to assess the overall L/D changes. This is best seen on a "powered polar." At vectored conditions, the powered polar comparison represents the external aerodynamics (including any vector-induced effects) and the components of the gross thrust in the lift and drag direction (including any C_{F_g} loss due to vectoring).

For all nonaxisymmetric nozzles tested, vectoring provided improvement over the unvectored powered polar at all positive thrust-vector deflection angles. The polar improvements at untrimmed conditions are typified by the VIP nozzle data shown in Fig. 8, where polar crossovers are indicated at succeedingly higher lift coefficients as vector angle is increased. The polars were improved significantly at angles of attack above the wing separation onset point, which was between $\alpha = 6$ and 8 deg for the symmetrical wing tested. This is because the incremental induced lift at all angles of attack is

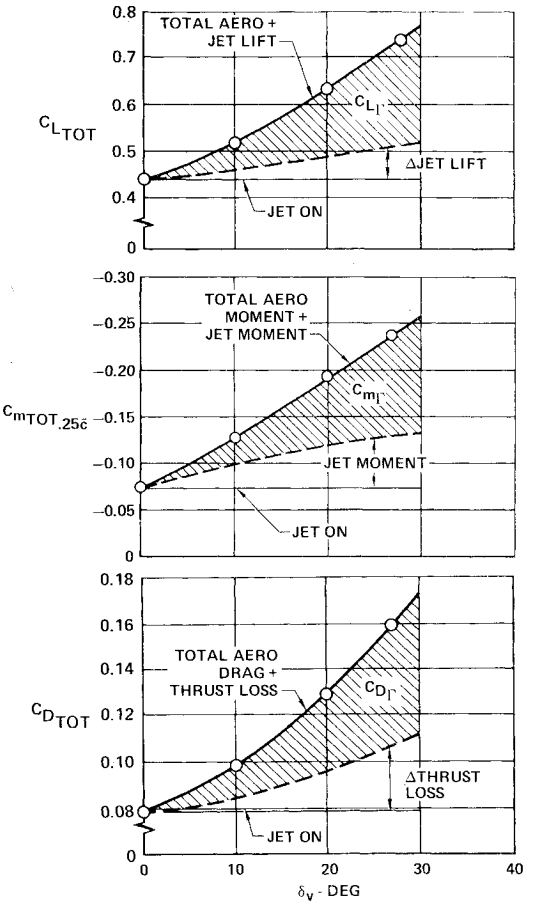

Fig. 7 Effects of vectoring on lift, drag, and pitching moment (GE 2-D C-D, low Mach A/B power, Mach 0.9, $\alpha = 8$ deg, $NPR = 5$, $C_T = 0.17$).

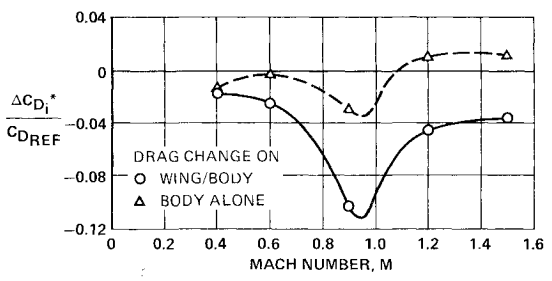

Fig. 6 Transonic induced drag improved (ALBEN installation, low Mach A/B power, operating NPR).

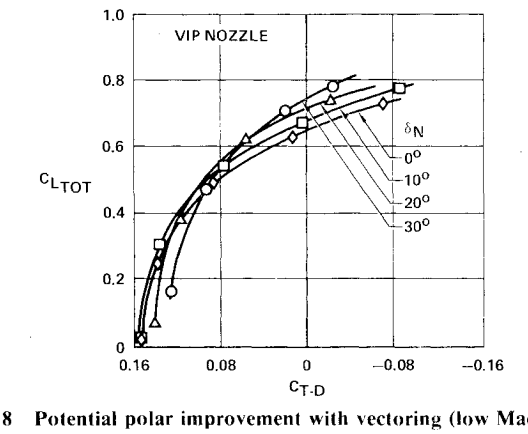

Fig. 8 Potential polar improvement with vectoring (low Mach A/B power, Mach 0.9, $NPR = 5$, uncambered wing, untrimmed).

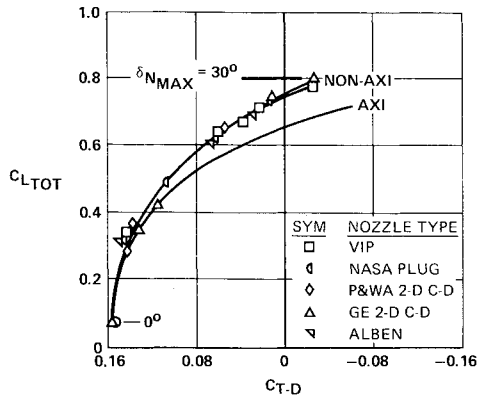

Fig. 9 Optimum vectoring (low Mach A/B power, Mach 0.9, *NPR* = 5, uncambered wing, untrimmed).

an increased circulation effect, with drag increases occurring without significant separation.

An interesting aspect is that the optimum powered polar, defined by the locus of maximum thrust minus drag, was essentially the same for all nonaxisymmetric nozzles. This is illustrated in Fig. 9, where data points near optimum for all five nozzle types are compared to the axisymmetric baseline.

The polar improvements presented in Figs. 8 and 9 reflect only the potential of thrust vectoring, since trimming of the vector-induced and direct jet moments could not be accomplished on the Test Pod arrangement. These untrimmed data must be used in a vehicle system evaluation to ascertain the vectoring payoff at trimmed conditions.

Empirical Correlations

Generalized correlations of the induced effects were formulated to provide design data applicable to other configurations. These correlations, which are detailed in the program final report,[8] were developed by considering the similarities of the vectored jet to deflection of a partial span trailing-edge flap on a wing. The deflected jet acts generally like a flap in that the circulation about the wing is increased locally by the jet sheet. Unlike the flap, however, the vectored jet has a variable penetration depth, or effective length, which is dependent upon power setting, nozzle pressure ratio, and Mach number.

Considering the analogy to flap behavior, the induced lift increments were correlated with nondimensionalized terms defining the direction of the deflected jet flow, the effective length of the deflected jet relative to the local wing chord, the height of the jet exit, and the extent of the wing influenced by the deflected jet. The induced lift correlation for all nozzles (Fig. 10) resulted in excellent agreement with measured aerodynamic lift increments.

A regression analysis technique was used to determine the constant K_L and exponents A, B, and C which gave the best correlation of the data (see Table 3). The terms defining the effective length of the deflected "jet flap" combine the effects of *NPR*, Mach number (included in the K_L value), and the jet exit thickness or height h_N (related to power setting). The term

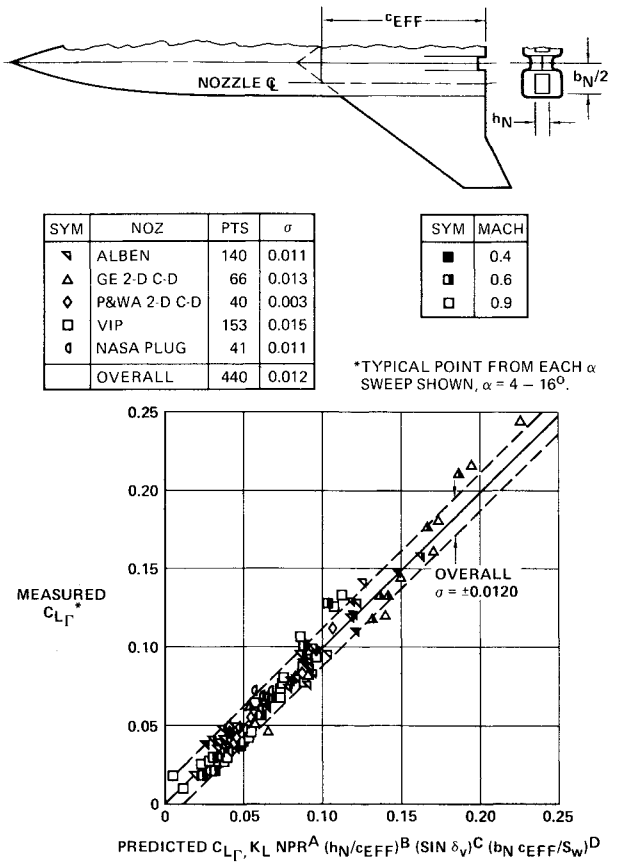

Fig. 10 Correlation of thrust vector-induced lift.

which accounts for nozzle spanwise location and aspect ratio ($b_N c_{EFF}/S_w$) was not a test variable. Thus, the exponent D could not be determined by regression analysis. However, this term is analogous to the affected wing area ratio in the widely used adjusted gain factor correlation,[13] where an exponent of 1.0 was used.

The induced pitching moment would be expected to relate directly to the induced lift, based on the unseparated flap analogy. This was indeed true for all nozzles, independent of thrust-vector angle, power setting, *NPR* and α. These results are shown in Fig. 11 and can be used to determine the magnitude of C_{m_Γ} as well as the effective point of application (X_Γ) of the induced lift relative to the 25% location of the effective wing section chord upstream of the nozzle (c_{EFF}). The 25% c_{EFF} location was arbitrarily chosen for data correlation purposes and allows application to other nozzle spanwise locations or wing geometries. The major constraint in application of the data is a nozzle exit location at the wing trailing edge.

Thrust-vector-induced drag increments would also be expected to correlate with the vector-induced lift, based upon drag-due-to-lift theory. If the assumption is made that the thrust-vector-induced drag increment C_{D_Γ} is primarily an

Table 3 Summary of constants in thrust vector-induced lift correlation

	Exponent values				K_L values		
Nozzle	*A*	*B*	*C*	*D*	Mach 0.4	Mach 0.6	Mach 0.9
ALBEN	0.69	0.69	1.33	1.0	3.90	2.45	1.50
P&WA 2-D C-D	0.69	0.69	1.33	1.0		2.05	1.99
GE 2-D C-D	0.69	0.69	1.33	1.0		2.67	2.89
VIP	0.41	0	0	1.0	0.373	0.290	0.285
NASA plug	0.41	0	0.87	1.0		0.213	0.157

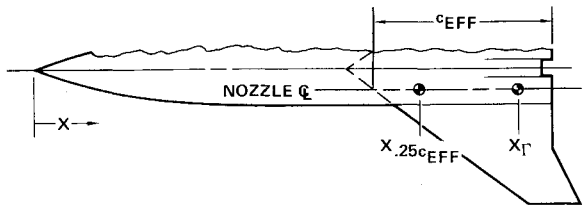

SYM	NOZ	PTS	σ
◹	ALBEN	140	0.0038
△	GE 2-D C-D	66	0.0038
◇	P&WA 2-D C-D	40	0.0016
□	VIP	153	0.0038
◖	NASA PLUG	41	0.0018
	OVERALL	440	0.0035

SYM	MACH
■	0.4
◨	0.6
□	0.9

*TYPICAL VALUES FROM EACH α SWEEP SHOWN.

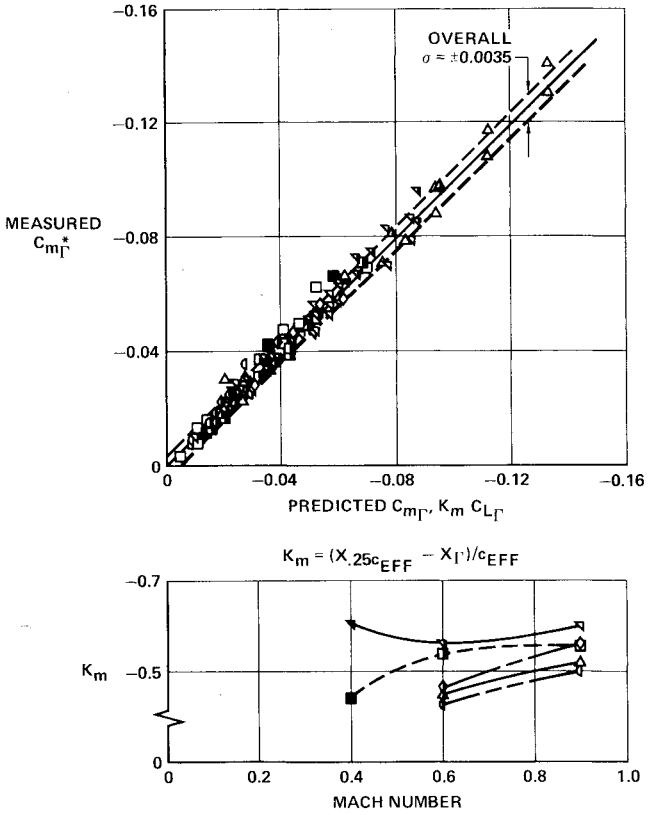

Fig. 11 Correlation of thrust vector-induced pitching moment.

SYM	NOZ	PTS	σ
◹	ALBEN	184	0.0036
△	GE 2-D C-D	84	0.0053
◇	P&WA 2-D C-D	51	0.0016
□	VIP	197	0.0027
◖	NASA PLUG	53	0.0019
	OVERALL	569	0.0034

SYM	MACH
■	0.4
◨	0.6
□	0.9

*TYPICAL POINT FROM EACH α SWEEP SHOWN.

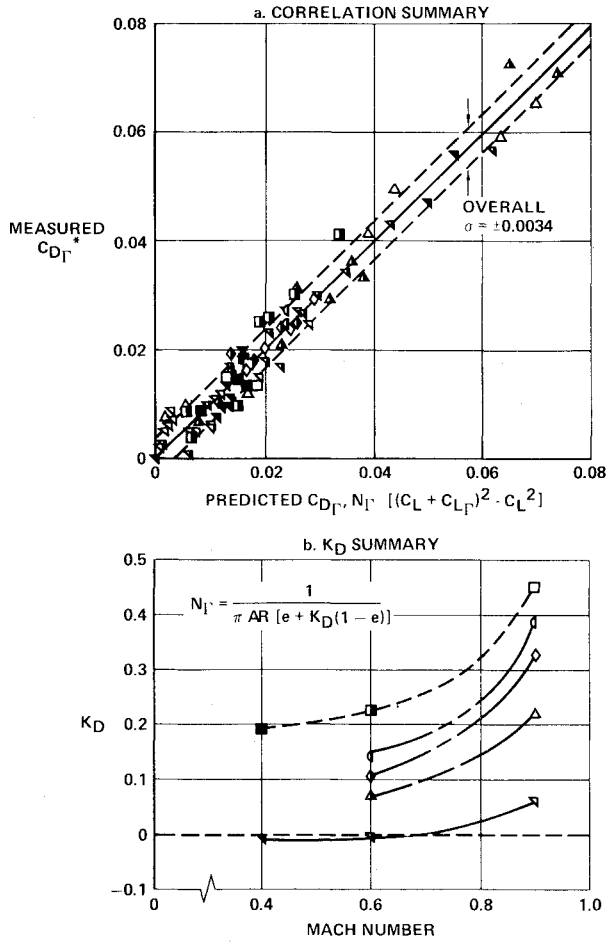

Fig. 12 Correlation of thrust vector-induced drag.

increased circulation effect and occurs with minimum flow separation, the standard drag-due-to-lift equation can be modified as follows to express C_{D_Γ} for the tested uncambered wing configuration.

$$C_{D_\Gamma} = \Delta C_{D_i} = N_\Gamma [C^2_{L_{(\delta_v = x)}} - C^2_{L_{(\delta_v = 0\,\text{deg})}}] \quad \text{(constant } \alpha)$$

Expressing $C_{L_{(\delta_v = 0\,\text{deg})}}$ simply as C_L, and recognizing that $C_{L_{(\delta_v = x)}} = (C_L + C_{L_\Gamma})$, this equation can be written as

$$C_{D_\Gamma} = N_\Gamma [(C_L + C_{L_\Gamma})^2 - C_L^2].$$

In this equation, C_L is the unvectored lift coefficient at any α, and N_Γ is the effective induced drag constant. In order to obtain N_Γ values from the data base representative of a complete configuration, the C_L values used in the correlation were obtained by increasing the measured aftbody/wing lift coefficient by an estimated lift increment for the nonmetric forebody. This technique resulted in excellent correlation of thrust vector induced drag increments, as summarized in Fig. 12, independent of angle of attack or thrust-vector angle. The good correlation accuracy at all tested angles of attack indicates that the efficiency losses normally associated with wing separation at high α do not affect thrust-vector-induced drag significantly.

The induced drag correlation was extended by modifying the conventional induced drag relationship so that the vectoring results could be applied to other wing characteristics on similar configurations. This was done by considering N_Γ to be analogous to the conventional definition for N, i.e., $N_\Gamma = 1/(\pi A R e_\Gamma)$, where e_Γ is the effective wing/body efficiency for the thrust vector-induced drag increment. The modification was to express e_Γ in terms of the unvectored wing/body efficiency e (from a jet-off polar at angles of attack below wing separation) and a vectoring efficiency factor K_D as follows:

$$e_\Gamma = e + K_D(1 - e)$$

The K_D values from the wind tunnel data were determined by a linear regression analysis technique and are shown in Fig. 12b.

Considering the above expression for e_Γ, it can be seen that as K_D varies from 0 to 1, e_Γ varies from a value equal to the

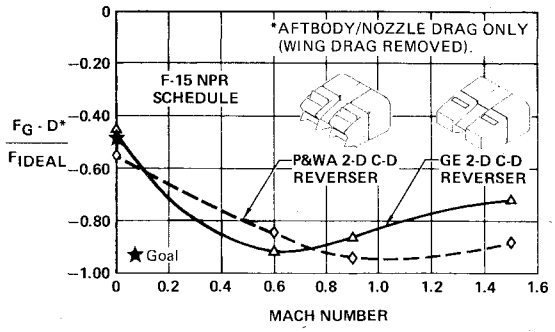

Fig. 13 Reverser performance goals achieved, (dry power, $\alpha = 0$ deg).

PERFORMANCE CATEGORY	COMPARISON BASIS (DESIGN NPR)	ALBEN	VIP	2-D C-D	
				GE	P&WA
INSTALLED ($\alpha = 0^o, \delta_N = 0^o$)					
• DRY (MACH 0.9)	$\frac{\Delta(F_g - D)}{F_{IDEAL}}$ ~% (1)	+0.2	−0.8	−2.8	−3.4
• LM A/B (MACH 0.9)		+1.2	+0.3	+0.3	−0.8
• LM A/B (MACH 1.5)		+2.0	+2.8	+0.1	−0.2
MANEUVER (MACH 0.9)					
• UNVECTORED	$\frac{\Delta C_{T\text{-}D}}{C_{D_{REF}}}$ ~% (2)	+13	+ 7	−13	− 5
• VECTORED (OPT δ_V)		+15	+15	+12	+12
REVERSE ($\alpha = 0^o$)					
• STATIC	$\frac{F_g - D}{F_{IDEAL}}$			−0.4	−0.5
• IN-FLIGHT (MACH 0.9)				−0.9	−0.9

(1) Δ FROM AXI BASELINE
(2) Δ FROM AXI AT $\alpha = 8^o$, CONSTANT $C_{L_{TOT}}$ (UNTRIMMED), $C_{D_{REF}}$ FOR TYPICAL ADVANCED FIGHTER AT $\alpha = 8^o$

Fig. 14 Summary of wind tunnel test results.

basic efficiency of the wing body (e) to a value of 1.0, which corresponds to the minimum possible drag-due-to-lift. Thus, K_D represents the degree to which vectoring can provide improvements in incremental drag-due-to-lift. However, even if $K_D = 0$ (such as for the ALBEN) and vectoring does not show improvements over the unvectored polar below wing separation, the overall polar above separation should be improved because the efficiency of the incremental L/D due to vectoring remains unchanged at the higher angles of attack.

Reverser Installed Performance

Thrust reversing is an effective means of improving landing performance (reduced ground roll), ground operating characteristics (less brake wear), and in-flight deceleration. Reverser installed performance at dry power was measured for both the GE and P&WA 2-D C-D nozzles at simulated sea level static and in-flight conditions. A reverser thrust efficiency ($F_{g_{rev}}/F_{ideal}$) goal of -0.5 was established for static conditions. The reverser performance goals were achieved for static conditions (Fig. 13), with the reverser effectiveness nearly doubled at Mach 0.9. The increase in efficiency with Mach number is due primarily to the high base drags developed on the rear of the reverser flap.

Summary

The aerodynamic performance characteristics of five different nonaxisymmetric nozzle concepts were evaluated experimentally for unvectored, vectored, and reverse thrust conditions in the PWT-16T tunnel at AEDC. The wind tunnel test results are summarized in Fig. 14.

Installed performance at unvectored conditions for the complete wing/aftbody varied considerably, depending upon power setting and nozzle type. At dry power, essentially equivalent performance was observed for the external expansion ALBEN and VIP nozzles. The poorer performance for the 2-D C-D designs was attributed to higher boattail and interfairing drag levels.

At subsonic afterburning conditions, installed performance of all configurations was almost equal. At supersonic afterburning, the external expansion ALBEN and VIP nozzles again were distinctly superior, probably due to improved area distributions.

A large difference in transonic maneuver performance was observed for unvectored conditions. However, nearly equal performance resulted with optimum vector angle settings, based on the untrimmed powered polars. The external expansion nozzles exhibited the highest performance unvectored, with favorable wing/body interactions contributing to lower transonic drag-due-to-lift. Optimum vectoring improved thrust-minus-drag for all nozzles, with the greatest improvement observed for the 2-D C-D nozzles.

Useful correlations of the thrust vector-induced lift, drag, and moment were derived in a form for generalized application. These correlations provide valuable insight into the L/D improvements achievable with vectoring.

High reverse thrust performance was measured for the GE and P&WA 2-D C-D test configurations. Reverser performance effectiveness was nearly doubled at Mach 0.9, compared to static conditions.

Acknowledgment

This research was conducted under USAF Contract F33615-76-C-3019.

References

[1] Willard, C.M., Capone, F.J., Konarski, M., and Stevens, H.L., "Static Performance of Vectoring/Reversing Non-Axisymmetric Nozzles," *Journal of Aircraft*, Vol. 16, Feb. 1979, pp. 116-123.

[2] Maiden, D.L., "Performance of an Isolated Two-Dimensional Variable-Geometry Wedge Nozzle with Translating Shroud and Collapsing Wedge at Speeds Up to Mach 2.01," NASA TN D-7906, 1975.

[3] Martens, R.C., "F-15 Nozzle/Afterbody Integration," *Journal of Aircraft*, Vol. 13, May 1976, pp. 327-333.

[4] Capone, F.J. and Maiden, D.L., "Performance of Twin Two-Dimensional Wedge Nozzles Including Thrust Vectoring and Reversing Effects at Speeds Up to Mach 2.20," NASA TN D-8449, 1977.

[5] Capone, F.J., "Supercirculation Effects Induced by Vectoring a Partial-Span Rectangular Jet," *Journal of Aircraft*, Vol. 12, Aug. 1975, pp. 633-638.

[6] Capone, F.J., "The Effects on Propulsion-Induced Aerodynamic Forces of Vectoring a Partial-Span Rectangular Jet at Mach Numbers From 0.4 to 1.2," NASA TN D-8039, 1975.

[7] Hiley, P.E., Wallace, H.W., and Booz, D.E., "Non-Axisymmetric Nozzles Installed in Advanced Fighter Aircraft," *Journal of Aircraft*, Vol. 13, Dec. 1976, pp. 1000-1006.

[8] Hiley, P.E., Kitzmiller, D.E., and Willard, C.M., "Experimental Evaluation of Non-Axisymmetric Exhaust Nozzles," McDonnell Aircraft Co., AFFDL-TR-78-185, Dec. 1978.

[9] Lander, J.A., Nash, D.O., and Palcza, J.L., "Augmented Deflector Exhaust Nozzle (ADEN) Design for Future Fighters," AIAA Paper 75-1318, Anaheim, Calif., Sept. 1975.

[10] Woodrey, R.W., Whitten, P.D., Smith, D.W., and Bradley, R.G., "An Experimental Investigation of a Vectored-Engine-Over-Wing Powered-Lift Concept," General Dynamics Corp., AFFDL-TR-76-92, Sept. 1976.

[11] Rosenthal, G., "Advanced Fighter Technology Integration (AFTI) Phase 1," Fairchild-Republic Co., AFFDL-TR-75-87, Aug. 1975.

[12] "USAF Stability and Control DATCOM (Section 6)," McDonnell Aircraft Co., AFFDL-TR-60-261, Jan. 1974.

[13] Sedgewick, T.A., "Investigation of Augmented Deflector Exhaust Nozzles Installed in Tactical Aircraft," Lockheed-California Co., AFFDL-TR-75-42, May 1975.